The crystal structure of a new calcium aluminate phase containing formate

Maria Chiara Dalconi[a], Gilberto Artioli[a], Norberto Masciocchi[b], Carlotta Giacobbe[c], Fabio Castiglioni[d], Giorgio Ferrari[d]

[a]Department of Geosciences and Circe Center, University of Padua, via G. Gradenigo 6, 35129 Padua, Italy
[b]Department of Science and High Technology and To.Sca.Lab., University of Insubria, Via Valleggio 11, 22100 Como, Italy
[c]European Synchrotron Radiation Facility, 71 Avenue Des Martyrs, Grenoble 38040, France
[d]Mapei S.p.A., via Cafiero 22, 20158 Milan, Italy

Abstract

A new calcium aluminate phase containing formate ions was synthesized and its crystal structure determined. This new phase is indicated as M-phase and was firstly observed in Portland cement pastes hydrated in presence of Ca-formate and in excess of water. The crystal structure of the M-phase was successfully solved in the *R-3* space group of the trigonal system on the basis of synchrotron X-ray single crystal diffraction data. The structural model was confirmed by Rietveld refinement of the powder diffraction data acquired on the synthesized pure sample. The crystal structure of the M-phase is similar to that of ettringite, being characterized by columns of AlO_6 octahedra alternating with groups of three edge-sharing CaO_7 polyhedra. The formate ions $(HCOO)^-$ share two oxygens with Ca polyhedra and are located in the interspace between the columns. The crystal structure of the M-phase testifies the strong interaction occurring between small organic molecules as formate and the calcium aluminate components of Portland cement.

1. Introduction

The use of organic admixtures to tailor the performance of concrete is a consolidated practice whose development dates back to the beginning of the 1950s [1]. Nowadays, the concrete industry uses a wide range of admixtures to accelerate or retard setting, to modify the rheological behaviour, to entrain air or to control the hardening process. Calcium formate belongs to the category of non-corrosive accelerators of cement setting and hardening and it is extensively used in prestressed and reinforced concrete applications [2].

It is known that calcium formate induces an acceleration of C_2S and C_3S hydration at early stages leading to a more rapid development of calcium silicate hydrate (C-S-H)

and consequently reducing the setting time of the cement paste [3,4]. The effect on calcium silicates is attributed to the higher diffusion rate of (HCOO)– ions which facilitate the dissolution of C_3S and C_2S [5,6]. A different interpretation was proposed by Lota [7] who observed that calcium formate is likely reacting with alkalis in the pore solution precipitating $Ca(OH)_2$ (CH in cement-chemistry notation). The early precipitated CH acts as nucleation seeds thus promoting the further precipitation of CH. Lota's hypothesis is based on the assumption that formate ions in solution combine with alkali to precipitate K- or Na-formate and the remnant Ca ions forms CH, however he did not consider the different solubility of the involved salts, being Ca-formate less soluble than K- or Na-formate. We can hypothesize that the excess of Ca ions released in solution by Ca-formate contributes to supersaturate the solution with respect to CH thus promoting the early precipitation of CH. Lota also observed a retarding effect of calcium formate at increasing additions, invoking a poisoning effect of formate incorporated onto C-S-H surface according to the model proposed by Jennings et al. [8]. Considering the different interpretations proposed in the literature, it emerges that a comprehensive understanding of the mechanism through which calcium formate operates is still to be accomplished. It is worth mentioning that the use of Ca-formate has been established on the basis of empirical optimization of the mixtures whereas the formate-cement interaction at molecular scale has not been deeply investigated.

Lota et al. [7] pointed the attention to calcium aluminate components of cement, suggesting that calcium formate readily reacts with C_3A to form $C_3A{\cdot}Ca(HCOO)_2{\cdot}nH_2O$, a calcium aluminate phase with a layered structure hosting formate ions in the interlayer (formate analogous of AFm phase). It is also suggested that, depending on the C_3A over $Ca(HCOO)_2$ ratio, a calcium aluminate phase containing six moles of formate ions ($C_3A{\cdot}3Ca(HCOO)_2{\cdot}nH_2O$) could form. This phase is described as the formate analogue of AFt phase [6,7]. These authors prospect the possible formation of calcium aluminate phases with formate ions, but no experimental data on their identification and characterization are reported. Going back to early literature on cement, Jones reports that needle-like crystals of $C_3A{\cdot}3Ca(HCOO)_2{\cdot}nH_2O$ were prepared through precipitation from calcium aluminate solution [9]. No crystal structure characterization by X-ray diffraction was performed at that time.

An extensive work on the synthesis and characterization of calcium aluminate phases containing formate was presented by H. Pöllmann and co-workers, who observed that, depending on the concentration of formate and condition of hydration, layered formate-AFm or solid solutions of AFm-phases containing formate or formate-AFt with an ettringite-like structure can crystallize [[10], [11], [12], [13]].

In this work we present the crystal structure of a calcium aluminate phase containing formate with structural features resembling that of an AFt-phase. This new phase has been indicated as the M-phase and was obtained from a Portland cement paste with the addition of a high dosage of calcium formate. The M-phase was additionally

obtained by reacting C_3A with calcium formate in excess of water. The crystal structure of the M-phase gives evidences of the strong interaction occurring between small organic molecules as formate and the calcium aluminate components of the cement phases. The proposed structural model of M-phase fills a gap in the knowledge of the possible hydration products of Portland cement and on their interaction with formate ions.

2. Material and methods

2.1. Synthesis

Ordinary Portland cement (CEM-I 52.5 R according to EN 197–1, mineralogical composition is reported in Table 1) was hydrated in excess of water (water/cement ratio of 3.67) with the addition of Ca-formate in high dosage (27.5 wt% by weight of cement). The obtained slurry was kept stirring during 24 h at a temperature of 60 °C. The proportions of cement, water and Ca-formate were calibrated to maximize the hydration degree of the cement paste during 24 h of mixing in excess of water. The initial goal was to produce a slurry composed of cement hydration products coexisting in a Ca-formate rich solution. X-ray diffraction data were acquired on the cement paste in excess of water, e.g. the slurry sample put in a sealed capillary and measured in transmission mode, and on the air-dried powder. No residues of clinker phases were detected indicating that the hydration of the cement paste was complete. The X-ray diffraction data collected on the slurry clearly revealed the presence of the Bragg reflections of the M-phase. The same diffraction peaks of M-phase were detected unaltered in the XRPD pattern measured on the air-dried sample, thus we could exclude any significant effect of the drying process on the stability of the M-phase. As later discussed, tiny single-crystal samples of the M-phase were found within the air-dried cement paste and isolated under a microscope.

Mineral phase	% wt
C_3S	57,2
C_2S	12,9
C_3A_{cub}	5,9
C_3A_{ort}	3,7
C_4AF	4,7
CaO	0,1
Periclase (MgO)	1,3

Gypsum ($CaSO_4*2H_2O$)	1,0
Bassanite ($CaSO_4*0,5H_2O$)	3,7
Anhydrite ($CaSO_4$)	<0,1
Arcanite (K_2SO_4)	1,3
Aphthitalite ($NaK_3(SO_4)_2$)	0,4
Portlandite ($Ca(OH)_2$)	1,2
Calcite ($CaCO_3$)	6,5

Table 1. Mineralogical composition of CEM-I 52.5 R used in this work.

Once the composition (and structure) of the M-phase were determined by single-crystal diffraction studies (vide infra), a sizable batch of polycrystalline M-phase deliberately was synthesized by reacting cubic C_3A (Mineral Research Processing) with Ca-formate (Sigma-Aldrich) in deionized water at temperature of 70 °C according to a C_3A:$Ca(HCOO)_2$ molar ratio equal to 1:3 (Table 2). The molar ratio was selected on the basis of the phase composition of M-phase as derived by single-crystal structure determination, which indicated a phase stoichiometry with 3 mol of formate and 1 mol of aluminium. The suspension was kept stirring for 24 h and then filtered, washed with deionized water and dried in a forced air cabinet at 50 °C. By the Quantitative Phase Analysis method encoded in the Rieveld refinement procedure, the final powder sample was found to be composed by more than 90 wt% of the M-phase and, from here on, is indicated as *pure M-phase*. A sample of pure M-phase was exposed to an atmosphere 1% CO_2-rich at 60% relative humidity for 7 days. Diffraction data collected on the M-phase after CO_2 exposure did not revealed any change in sample phase composition, indicating that M-phase is not sensitive to carbonation at ambient condition.

C_3A (g)	$Ca(HCOO)_2$ (g)	H_2O (cc)	Mixing temp. (°C)	Mixing time (h)
2	2.89	40	70	24

Table 2. Proportions and conditions of synthesis for pure M-phase.

2.2. Single crystal X-ray diffraction

Micro-focussed single crystal diffraction data were collected at the nanoscope station of ID11 beamline (ESRF, Grenoble, France) [13] using a monochromatic beam (60 keV, wavelength = 0.2065 Å, relative bandwidth $\Delta\lambda/\lambda \sim 10^{-3}$) produced by a bent Si(111) Laue–Laue double-crystal monochromator. Acicular crystals of the M-phase

were isolated from the hydrated cement paste by hand picking. A selected crystal 2 × 2 × 1 μm in size was mounted under an optical microscope and glued onto a MiTeGen microloop. After positioning the preselected crystal by optical alignment, it was centred in a beam of 1 μm diameter with the help of the standard deviation signal recorded by the diffraction camera. A series of images (1440) have been recorded while the sample was rotating through 360° (with a resulting step-size per image of 0.25°) with an exposure time of 0.35 s using a CCD Frelon4M detector (ESRF, Grenoble, France) (2048 × 2048 pixels of 50 × 50 μm).

Images were then converted into the "Esperanto" format using an in-house software (FREAC), an open source program written in Python and C which converts ID11 EDF images into the packed ESPERANTO format accepted by the commercial software CrysAlisPro [14]. The tool modifies the values of the φ angle inside the header of each image of a series. Note that the pure ω scan at the beamline (equipped with one circle only) is interpreted in CrysAlisPro as a φ scan. To do so, the first and last file of an image series needs to be selected as well as a starting value for the φ angle and a step width 'Delta PHI' of the step scan. CrysAlisPro allowed the indexing of the phase and intensities extraction. The preliminary structure was solved using the direct methods approach implemented in SHELXL [15]. During the data collection, crystallites proved to be highly sensitive to beam exposure, so that the last frames of the data collection were devoid of diffraction spots. However, the data quality allowed to obtain approximate unit cell parameters and a preliminary structural model that has been used as input for the Rietveld refinement that enabled to depict the final structure.

2.3. X-ray powder diffraction

The air-dried samples were gently disaggregated with a mortar and pestle for X-ray Powder Diffraction (XRPD) measurements and no sieving was applied. The diffraction pattern of the hydrated cement paste was collected using a X'PertPro MPD diffractometer (Malvern-Panalytical) equipped with a Co tube, Bragg-Brentano HD optic module, Soller slits with 0.04 rad aperture and X'Celerator detector. Data were collected in the 5°-80° 2θ range, 0.017° step size, counting an equivalent time of 60 s per step. The pure sample of the M-phase was measured using a X'PertPro MPD diffractometer in Bragg-Brentano geometry, with a Cu tube, incident ad diffracted beam Soller slits of 0.02 rad and a PIXcel2D detector. The details of data collection are reported in Table 3. Rietveld refinement of the pure M-phase was performed with Topas (v2.1) using a starting structural model as derived by single-crystal structure determination. The peak profile was fitted by applying the fundamental parameter approach. Both Gaussian and Lorentzian contributions were used to describe the sample-related peak broadening and the background was modelled with Chebychev polynomials of 7th order. The March-Dollase approach was used to correct effects of preferred orientation according to the (0001) crystallographic direction. Atomic coordinates were refined starting from the values determined by single crystal

structure solution, and an overall isotropic atomic displacement parameter (B_{iso} = 1 $Å_2$) was used.

Molecular formula	**$Ca_3Al(HCOO)_3(OH)_6$**
Wavelength (Å)	Cu $Kα_{1,2}$
Starting angle (°2θ)	5
Final angle (°2θ)	130
Step size (°2θ)	0.013
Equivalent counting time per step (s)	998
Weight amount (%)	92.3 (2)
Space group	R-*3*
a (Å)	13.7387 (1)
c (Å)	10.5894 (2)
V ($Å_3$)	1730.99 (4)
R_{Bragg}[a]	3.65
R_{exp}[a]	2.72

R_p[a]	3.84
R_{wp}[a]	5.05
GOF[a]	1.86

[a] Rietveld refinement agreement indices as defined in Topas v. 2.1 (Bruker AXS 2000).

Table 3. Details of diffraction measurement and Rietveld refinement data of M-phase.

2.4. Raman spectroscopy

Micro-Raman spectroscopy was conducted on a dried sample of the hydrated cement paste and on the pure M-phase using a Thermo Scientific DXR Micro-Raman spectrometer equipped with a 532 nm laser, a grating of 900 lines/mm and a spectrograph aperture of 50 μm. Spectra were selectively acquired pointing on particles with different morphologies. The laser power was kept as low as 5 mW to avoid damages of the sample surfaces. For Raman measurements, the air-dried samples were disaggregated with a spatula and deposited on a glass slide.

2.5. Scanning electron microscopy

Backscattered and secondary electron images of a dried sample of the hydrated cement paste were collected using a CamScan MX 2500 scanning electron microscope (SEM) coupled to an EDS spectrometer equipped with a LaB_6 cathode and operating at an accelerating voltage of 20 kV. The dried sample was dispersed on a conductive tape and sputtered with carbon.

3. Results and discussion

3.1. Phase identification

The X-ray diffraction pattern of the dried cement paste is reported in Fig. 1. Distinct diffraction peaks (d-spacings of 6.87 Å, 5.19 Å, 4.86 Å and 4.14 Å) were detected not matching any of the known phases comprised in PDF-2 (release 2002) or COD (release 2014) databases. Other identified crystalline phases were ettringite, portlandite (CH in cement notation), calcite and a minor amount of periclase. No

residual clinker phases were detected, indicating that the starting cement powder was totally hydrated. Calcium silicate hydrate (C-S-H- according to cement notation), which is the main hydration product of Portland cement [16], is poorly crystalline and it contributes to the diffraction pattern as an amorphous component. The wide hump between 28° and 42° 2θ (Fig. 1) was related to the amorphous contribution of C-S-H. The suite of identified phases is consistent with an ordinary Portland cement paste that has completely hydrated. The presence of any polymorph of Ca-formate, which possibly re-precipitated from cement pore solution during the drying process, was excluded on the basis of the diffraction data. Ca-formate polymorphs are typically crystalline and clearly identifiable by X-ray powder diffraction [14]. Considering the high dosage of Ca-formate added to the cement mixture, the unknown phase was at first ascribed to a hypothetical phase in which formate ions played a pivotal role. In the literature of cement, we found indications that calcium formate likely reacts with C_3A to form $C_3A{\cdot}Ca(HCO_2)_2{\cdot}xH_2O$ and $C_3A{\cdot}3Ca(HCO_2)_2{\cdot}xH_2O$ which are the formate analogous of AFm and AFt phases respectively [6,7,[10], [11], [12]]. The indexed patterns of formate-AFm ($C_3A{\cdot}Ca(HCOO)_2{\cdot}11H_2O$, reference code 00-041-0725) and formate-AFt ($C_3A{\cdot}3Ca(HCOO)_2{\cdot}32H_2O$, reference code 00-041-0726), are reported in the PDF-2 database but did not match the diffraction peaks observed in our sample. It is to note that the reference patterns of formate-AFm and formate-AFt refer to phases synthesized at 25 °C whereas the cement sample was hydrated at 60 °C. It is likely that the higher temperature of synthesis affected the content of water molecules in the possibly formed formate –AFt (reference code 00-041-0726). Nonetheless, the observed diffraction peaks could not be matched by formate-AFt reference pattern even considering a shrinkage of the unit cell volume related to a minor water content.

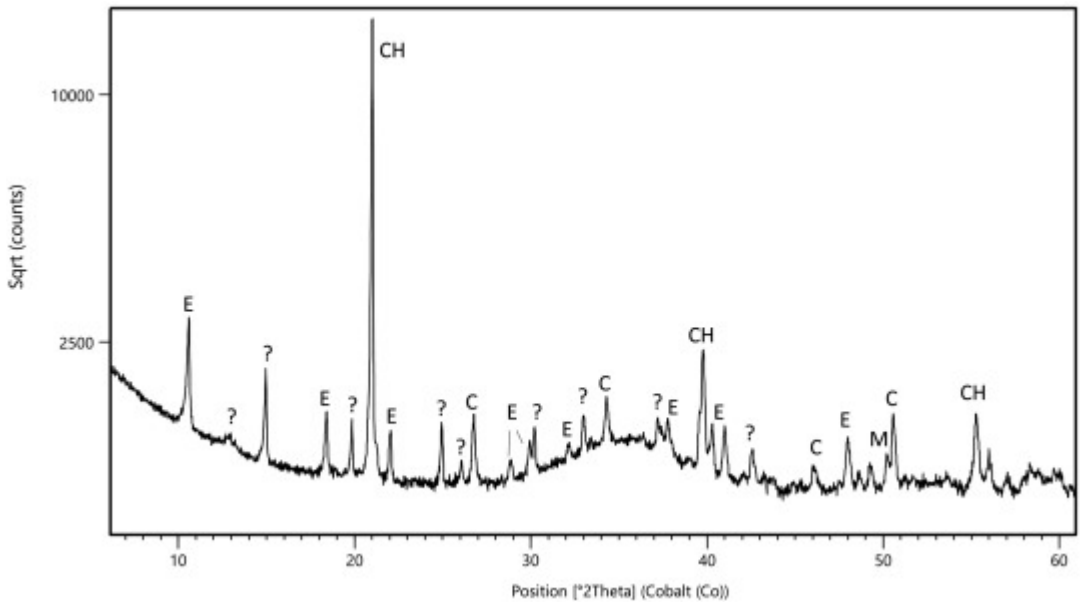

Fig. 1. Selected 2θ range of the diffraction pattern of the hydrated cement paste (dried powder sample). Main diffraction peaks are labelled as E = ettringite, CH = portlandite, C = calcite, M = periclase,? = unknown phase.

3.2. Raman spectroscopy

The dried cement paste was investigated by Raman spectroscopy pointing the laser on particles with different morphologies. Fig. 2 displays the Raman spectrum collected on a sample area rich in needle-like particles. The measured spectrum of Ca-formate and the reference spectrum of calcite (RUFF ID R050009) are reported for comparison. In the medium Raman-shift region, the strongest bands at 1403 cm^{-1} and 1367 cm^{-1} can be assigned to the internal vibrations of the formate ion [18]. The occurrence of these bands supports the hypothesis that the needle-like particles are strongly related to the formate ion. The broad band at 529 cm^{-1} likely originates by the Raman active vibrations of the AlO_6 group [19]. The sharp band at 1085 cm^{-1} and 989 cm^{-1} can possibly be assigned to the presence of calcite and ettringite respectively in the investigated area. Calcite and ettringite were clearly detected by X-ray diffraction data. The spot size of the laser beam (2 × 2 μm) encompassed a sample volume larger than the acicular crystals, and the recorded Raman spectrum is expected to be the sum of contributions of multiple phases. The Raman spectrum collected on the pure M-phase is displayed in Fig. 2 and the main Raman bands are reported in Table 4. The Raman bands observed for the needle-like particles in the cement paste exactly correspond to those of the pure M-phase, thus confirming the assignment of these bands to the M-phase.

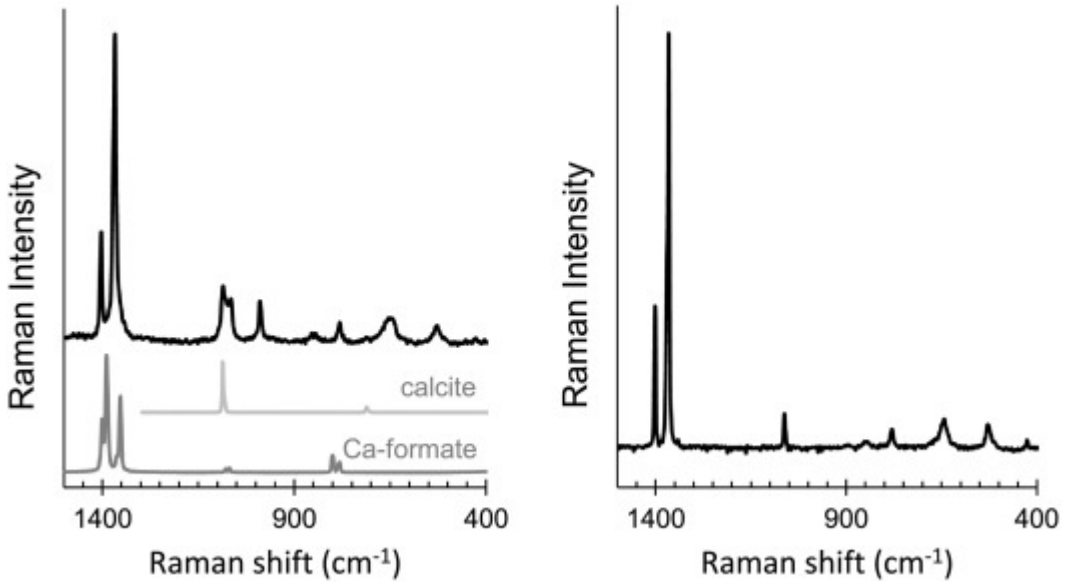

Fig. 2. Left: Raman spectrum in the range 1500 cm^{-1}–400 $cm^{-1}$of a selected area in cement paste. Reference Raman spectra of calcite and Ca-formate in the bottom part. Right: Raman spectrum of pure M-phase.

Band number	Band position (cm^{-1}), shape	Assignment
1	1402 vs	γ(CH) [formate]
2	1366 vs	ν(CO) [formate]
3	1062 m, s	γ(CH) [formate]
4	780 m, br	γ(CO) [formate]
5	643 m, br	
6	529 m, br	$[Al(OH)_6]$
7	427 w	

vs: very strong, m: medium, w: weak, br: broad; band assignment according to [18,19].

Table 4. Measured band positions in the range 1500 cm^{-1}–400 cm^{-1} of M-phase $Ca_3Al(HCOO)_3(OH)_6$.

3.3. Scanning electron microscopy

Fig. 3.a shows the secondary electron image of the dried cement suspension. Globular and needle-like structures are clearly visible. Fig. 3.b shows needle-like crystals that were separated from the dried cement paste by hand-picking, while Fig. 3.c presents needle-like structures obtained from the synthesis of pure M-phase. The selected crystals in Fig. 3.b are approximatively 12 × 1.5 μm and are covered by smaller particles. EDX analysis were executed on selected points of the elongated crystals. Calcium and aluminium were found as the main constituents, with minor amounts of silicon. Note that, in the presently used experimental set-up, oxygen and carbon signals cannot be determined. Among the hydration products detected by XRPD, it is reported in the cement literature that the crystalline phase exhibiting elongated crystals is ettringite, a calcium aluminate phase with sulfate (AFt). The hypothesis of ettringite crystals was discarded on the basis of EDX analysis that did

not detect any sulphur. It is to note that EDX analysis was conducted only on selected needle-like crystals picked up from the cement paste on the basis of their morphology. It was assumed that the elongated crystals correspond to the unknown phase (M-phase) detected by XRPD, and that this phase is a calcium aluminate containing formate ions, as indicated by Raman spectroscopy results. The globular particles rich in Ca and Si are referred to C-S-H. The tiny particles dispersed on the surface of elongated crystals are possibly C-S-H, thus explaining the minor Si detected by EDX. This hypothesis is supported by the absence of the globular structures in the pure M-phase of Fig. 3.c, indicating that they are a product of cement hydration.

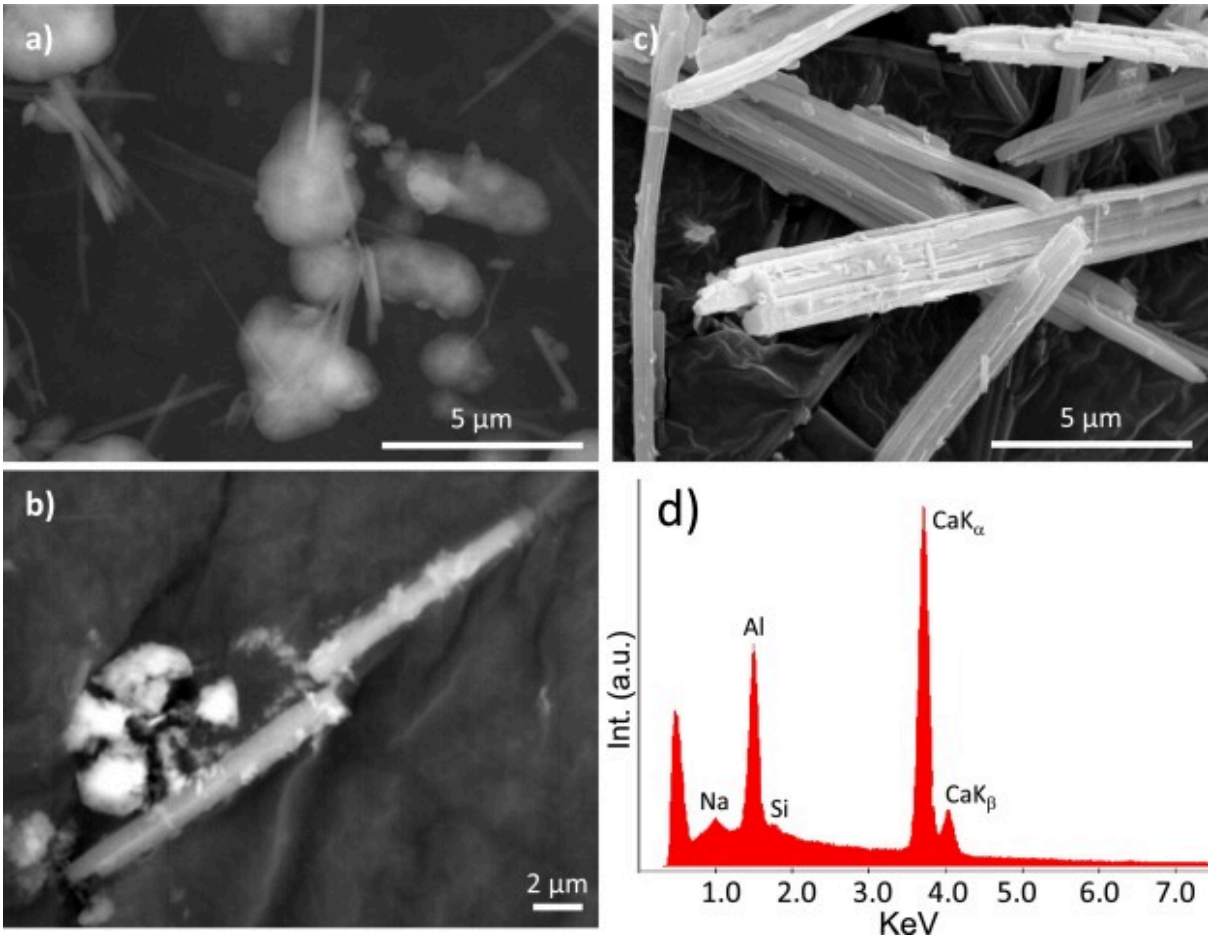

Fig. 3. Backscattered and secondary electron images of: a) globular structures and acicular crystals in dried cement paste (SE); b) needle-like crystals of M-phase separated from cement paste (BSE); c) needle like crystals obtained from the synthesis of pure M-phase (SE); d) point analysis EDX spectrum of acicular crystal in image b.

3.4. Crystal structure of M-phase

The crystal structure of the M-phase was solved in the trigonal system R-*3* space group on the basis of single crystal diffraction data. The derived molecular formula is

$Ca_3Al(HCOO)_3(OH)_6$ that can be expressed in cement notation as $C_3A{\cdot}3Ca(HCOO)_2{\cdot}6H_2O$. The tentative structural model derived from single crystal diffraction data was confirmed and refined by Rietveld analysis of powder diffraction data. Table 5, Table 6 report the unit cell dimensions and the atomic coordinates of the determined structure. Aluminium ions are located in two distinct crystallographic sites and are six-fold coordinated to oxygen atoms. Al octahedra alternate with groups of three Ca ions along the *c* crystallographic direction. Ca ions are 7-fold coordinated sharing part of their edges with Al octahedra. This arrangement of alternating Al and Ca polyhedra running parallel to one direction (Fig. 4, Fig. 5) can be described as columns analogous to that of the ettringite structure [20]. Differently from ettringite, the coordination of Ca ions is lowered to 7 forming an irregular polyhedron. A 7-fold coordination of calcium is a structural feature common to layered AFm-phases (e.g. monocarboalluminate) and Ca-formate. The columns are connected to each other through edge-sharing Ca polyhedra which thus form irregular chains intersecting near the Al octahedra. The formate ions are located in the intercolumn space bridging the Ca polyhedra. Each formate group shares one oxygen (O3) with one Ca ion and the other oxygen (O4) with two Ca ions. Hydrogen atoms (H1) of formate groups were placed according to geometric criteria. This structural arrangement of 7-fold Ca polyhedra bridged by formate groups which form monodentate ligands with Ca is similar to that of Ca-formate-alpha polymorph [21]. Contrary to Ca-formate, no chelate formates were detected.

Site	**Atom**	**Mult/Wyck.**	**S.O.F.**	***x/a***	***y/b***	***z/c***	**Beq/Å2**
Al1	Al	*3a*	1	0.0	0.0	0.0	1
Al2	Al	*3a*	1	0.0	0.0	0.5	1
Ca1	Ca	*18f*	1	0.17765(1)	0.0719(1)	0.2461(2)	1
O1	O	*18f*	1	0.0752(3)	0.1297(2)	0.1090(4)	1
O2	O	*18f*	1	0.0503(3)	0.9227(3)	0.3910(4)	1
C1	C	*18f*	1	0.3175(2)	0.3252(2)	0.5873(2)	1

H1	H	*18f*	1	0.32887	0.27031	0.62426	1
O3	O	*18f*	1	0.2199(10)	0.3041(11)	0.5849(12)	1
O4	O	*18f*	1	0.3334(3)	0.2590(3)	0.2157(4)	1

[a] 36 H of hydroxyl groups not located.

Table 5. Atomic coordinates, occupancies (S.O·F) and atomic displacement parameters of $Ca_3Al(HCOO)_3(OH)_6$[a] as derived by Rietveld refinement of XRPD data.

Atoms	**Distance Å**	**Atoms**	**Distance Å**
Al1-O1	1.932(3) x6	O1-O1	2.683(4)
Al2-O2	1.916(5) x6	O1-O1	2.781(7)
Ca1-O1	2.374(4)	O2-O2	2.650(9)
Ca1-O2	2.427(4)	O2-O2	2.769(7)
Ca1-O1	2.414(4)		
Ca1-O3	2.441(4)	Atoms	Angle
Ca1-O4	2.521(4)	O3-C1-O4	133°
Ca1-O4	2.407(4)	H1-C1-O3	115°
Ca1-O2	2.456(4)	H1-C1-O4	112°
C1-H1	0.929		
C1-O3	1.224(4)		
C1-O4	1.257(4)		

Table 6. Selected interatomic distances and angles of M-phase as determined by Rietveld structure refinement.

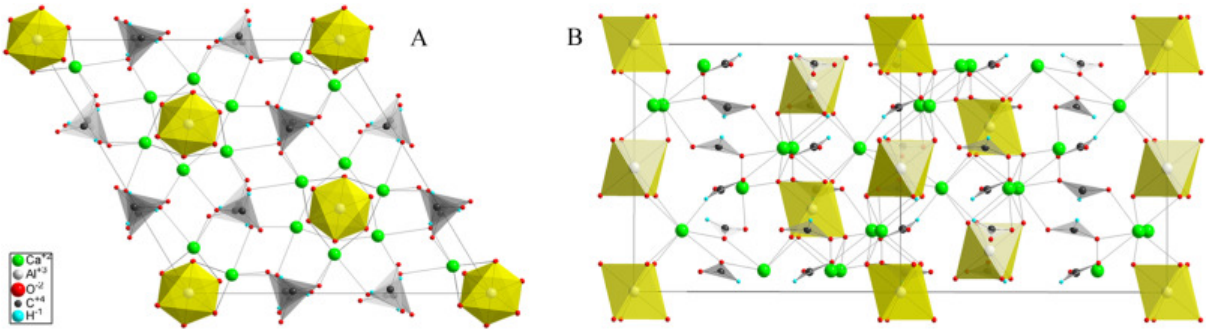

Fig. 4. Crystal structure of M-phase, viewed down the [0001] direction (A) and the [[11], [12], [13], [14], [15], [16], [17], [18], [19], [20]] direction (B).

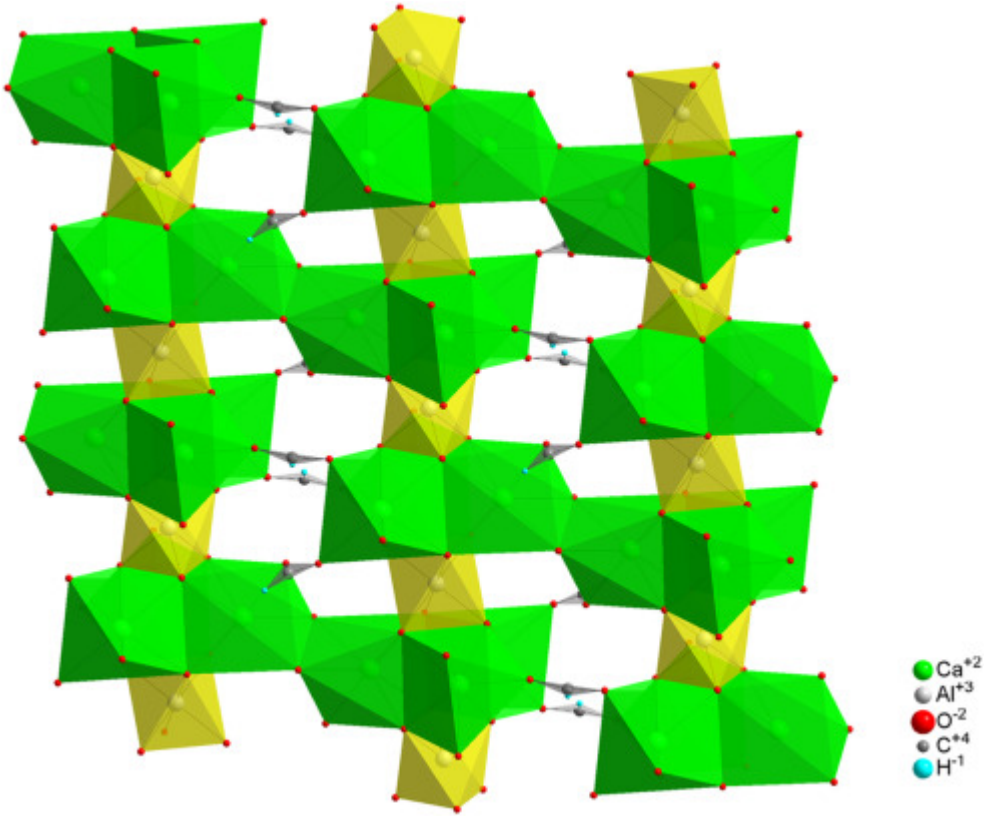

Fig. 5. The main structural motif of M-phase (columns), view down the [[11], [12], [13], [14], [15], [16], [17], [18], [19], [20]] direction.

Table 6 reports the more relevant interatomic distances. The two octahedral sites for Al are regular in shape and slightly differ in the mean Al—O distance, being 1.92 Å and 1.93 Å respectively. Within the octahedra, the O—O distances are shorter for the edges shared with Ca polyhedra. In the Ca polyhedron, the Ca—O distances range between 2.37 Å and 2.52 Å and are consistent with those of Ca-formate. Within the $(HCOO)^-$ groups, the C—O, C—H and O—O distances were restrained during the refinement. The presence of water molecules in the inter-columns space was excluded on the basis of void-space analysis performed with crystal structure visualization programs. Table 7 reports a brief comparison among the crystallographic features of M-phase, formate-AFt and ettringite. The structural similarity between M-phase and AFt-phases encompasses the columns of alternating

Al and Ca polyhedra running parallel to crystallographic *c* direction, but dissimilarly to ettringite or formate-AFt, the M-phase has a more compacted structure and no water molecules can be allocated in the space between the columns which are directly linked through formate groups and edge-sharing Ca polyhedra.

M-phase	**Formate-AFt**[a]	**Ettringite**[b]	
Molecular formula	$Ca_6(Al(OH)_6)_2(HCOO)_6$	$Ca_6(Al(OH)_6)_2(HCOO)_6\cdot(H_2O)_{26}$	$Ca_6(Al(OH)_6)_2(SO_4)_3\cdot(H_2O)_{26}$
Molecular formula in cement notation	$C_3A\cdot3Ca(HCOO)_2\cdot6H_2O$	$C_3A\cdot3Ca(HCOO)_2\cdot32H_2O$	$C_3A\cdot3CaSO_4\cdot32H_2O$
space group	R-*3*	P*31c*	P*31c*
a (Å)	13.739	10.907	11.260
c (Å)	10.589	21.231	21.480
Vol. ($Å_3$)	1730.99	2187.32	2358.53
density (g/cm_3)	2.18	1.88	1.76

a Data from PDF-2, reference code 00-041-0726.

b Data from [20].

Table 7. Comparison of crystallographic features of M-phase, formate-AFt and ettringite.

3.5. Rietveld refinement of pure M-phase

The powder diffraction data of the pure M-phase were analysed by the Rietveld method and Table 3 summarizes the obtained results. Fig. 6 shows the measured and calculated profile and their difference plot. The sample of pure M-phase contained minor amounts of monocarboaluminate (an AFm phase, 4.1 wt%), calcite (0.9 wt%) and aragonite (2.7 wt%). The diffraction peaks of these accessory phases did not severely overlap with the main signal of the M-phase. In the Rietveld refinement, the atomic coordinates of the initial single-crystal structural model were refined without applying any constraint. The refined interatomic distances are consistent with those of the starting model, thus validating the correctness of the structural model determined from single crystal method. Additionally, the agreement indices of the refinement with R_{wp} 5.05% and R_{Bragg} 3.65% corroborate the reliability of the structural model.

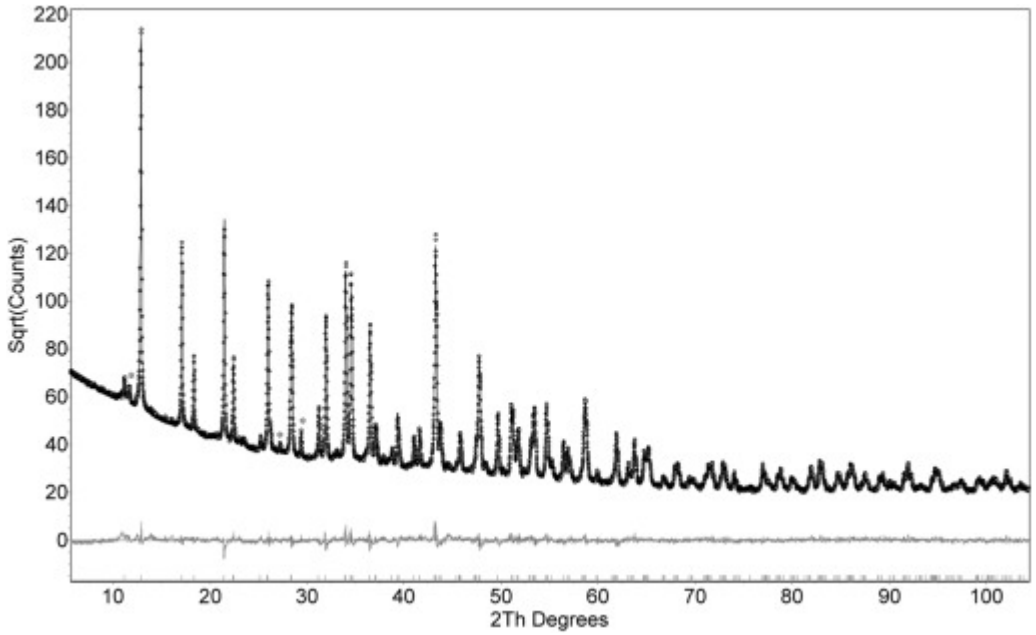

Fig. 6. Rietveld fit of M-phase. λ = Cu $K\alpha_{1,2}$ radiation. Solid line: calculated profile, crosses: measured profile, bottom line: difference curve (measured – calculated); *: diffraction peaks of accessory phases.

4. Conclusions

We described the synthesis and structure of a calcium aluminate phase containing formate ions. This phase has been indicated as the M-phase and its crystal structure shows features similar to ettringite, being characterized by columns of Al octahedra alternating with groups of three Ca polyhedra. Formate anions behave as carboxylate linking unit connecting Ca ions of adjacent columns. The columns are interconnected

also by edge-sharing Ca polyhedral. This causes the structure of M-phase being more compact than ettringite. The M-phase was observed in Portland cement paste hydrated with the addition of Ca-formate in high dosage. This new phase was also synthesized starting from C_3A and Ca-formate in due proportions and in excess of water at ambient atmosphere. Structure determination was achieved on the basis of single-crystal diffraction data using the high flux provided by a synchrotron source. The needle-like crystals isolated from the cement paste were too small for conventional single-crystal x-ray diffraction. The reliability of the proposed structural model was confirmed by Rietveld refinement performed on powder diffraction data of the deliberately synthesized pure M-phase. The crystal structure of the M-phase gives evidences of the strong interaction occurring between small organic molecules as formate and the calcium aluminate components of the cement phases, at least at the synthesis conditions adopted in this study. The high concentration of formate and hydration condition at 60 °C may have played a role in forming the M-phase instead of formate-AFt previously observed by Pöllmann. We cannot exclude that the synthesis condition under an ambient atmosphere (not CO_2-free atmosphere) may have affected the process too. Nonetheless, on the basis of single crystal diffraction data there was no direct evidence of the presence of CO_3 groups in the crystal structure. The proposed structural model of M-phase fills a gap in the knowledge of the possible hydration products of Portland cement and on their interaction with formate ions.

Acknowledgements

Michele Secco and Leonardo Tauro are acknowledged for their support during Raman and SEM measurements. This work was performed with financial support of the Mapei S.p.A-Unipd research agreement.

References

1. P. Aïtcin, R.J. Flatt
Science and Technology Of Concrete Admixtures
(first ed.), 59, Woodhead Publishing Series in Civil and Structural Engineering (2016)

2. P.K. Metha, P.J.M. Monteiro
Concrete – Microstructure, Properties, and Materials
(third ed.), McGraw-Hill (2006)

3. S. Gebler
Evaluation of calcium formate and sodium formate as accelerating admixtures for Portland cement concrete
ACI J. (1983), pp. 439-444

4. R. Rixom, N. Mailvaganam
Chemical Admixtures for Concrete
E & FN Spon, London (1999)

5. R. Kondo, M. Daimon, E. Sakai, H. Ushiyama
Influence of inorganic salts on the hydration of tricalcium silicate
J. Appl. Chem. Biotechnol., 27 (4) (1977), pp. 191-197, 10.1002/jctb.5020270128

6. M. Heikal
Effect of calcium formate as an accelerator on the physicochemical and mechanical properties of pozzolanic cement pastes
Cem. Concr. Res., 34 (2004), pp. 1051-1056,
10.1016/j.cemconres.2003.11.015

7. J.S. Lota, J. Bensted, P.L. Pratt
Hydration of class G oilwell cement at 20 °C and 5 °C with calcium formate
Proceedings of 21st International Conference on Cement Microscopy, Las Vegas, Nevada, USA (1999), pp. 160-179

8. H.M. Jennings, H. Taleb, G. Frohnsdorff, J.R. Clifton
Interpretation of the effects of the retarding admixtures on pastes of C3S, C3A plus gypsum and Portland cement
Proc. 8th Int, Congr. Chem. Cem., Rio de Janeiro, 3 (1986), pp. 239-243

9. F.E. Jones
The calcium aluminate complex salts
Proceedings of the Symposium on the Chemistry of Cements, Stockholm (1938), pp. 231-245

10. H. Pöllmann, S. Stöber
Hydration characteristics and new hydrates using organic additives (carboxylates & sulfonates)
Proceedings of the 10th International Congress on the Chemistry of Cement, Gothenburg (1997)
(3iii032, 8 pp)

11. H. Pöllmann, R. Kaden, S. Stöber
Crystal Structure and XRD Data of New Calcium Aluminate Cement Hydrates, Calcium Aluminates: Proceedings of the International Conference, Avignon
(2014), pp. 75-85

12. H. Pöllmann
Study of the hydration mechanisms and formation of new hydrates applying organic additives to the aluminate phase of cement
Proc. 11th Conf. on Cem. Micr. New Orleans (1989), pp. 287-305

13. J. Wright, C. Giacobbe, M. Majkut
New opportunities at the materials science Beamline at ESRF to exploit high energy nano-focus X-ray beams
Curr. Opin. Solid St. M., 100818 (2020),
10.1016/j.cossms.2020.100818

14. Rigaku Oxford Diffraction Ltd
CrysAlis PRO
Rigaku Oxford Diffraction Ltd., Yarnton, UK (2015)

15. G.M. Sheldrick
Crystal structure refinement with SHELXL
Acta Cryst, C71 (2015), pp. 3-8,
10.1107/S2053229614024218

16. H.F.W. Taylor
Cement Chemistry
(2nd edition), Thomas Telford, London (1997)

17. B.F. Mentzen, C. Comel
Comparative study of the polymorphic species of strontium and calcium formates. II. X-Ray diffraction
J. Solid State Chem., 9 (3) (1974), pp. 214-223,
10.1016/0022-4596(74)90077-2

18. R.S. Krishnan, P.S. Ramanujam
Raman spectrum of calcium formate
J. Raman Spectrosc., 1 (1973), pp. 533-538,
10.1002/jrs.1250010603

19. T. Runcevski, R.E. Dinnebier, O.V. Magdysyuk, H. Pollmann
Crystal structures of calcium hemicarboaluminate and carbonated calcium hemicarboaluminate from synchrotron powder diffraction data
Acta Cryst. B, 68 (2012), pp. 493-500,
10.1107/S010876811203042X

20. A.E. Moore, H.F. Taylor
Crystal structure of ettringite
Acta Cryst. B, 26 (1970), pp. 386-393,
10.1107/S0567740870002443

21. M.O. Bargouth, G. Will
Calcium formate Ca(HCOO)2 (neutron)
Cryst. Struct. Commun., 9 (1980), pp. 605-613